

An Algorithm for the Analysis of Inductive Antennas
of Arbitrary Cross-Section for Heating in the
Ion Cyclotron Range of Frequencies

by

Ira S. Lehrman* and Patrick L. Colestock

Plasma Physics Laboratory, Princeton University
Princeton, NJ 08544

MASTER

Abstract

The application of Ion Cyclotron Range of Frequency (ICRF) heating to near ignited plasmas will require launching structures that will be capable of withstanding the harsh plasma environment. The recessed antenna configuration is expected to provide sufficient protection for the structure, but to date no analysis has been done to determine if adequate coupling can be achieved in such a configuration. In this work we present a method for determining the current distribution for the antenna in the direction transverse to current flow and predict antenna loading in the presence of plasma. Antennas of arbitrary cross section are analyzed above ground planes of arbitrary shape. Results from ANDES, the ANTenna DESIGN code, are presented and compared to experimental results.

*Permanent Address: Grumman Aerospace Corporation, 105 College Rd. East,
Princeton, NJ 08540

EMB

I. Introduction

A key issue in the use of the fast magnetosonic wave for plasma heating applications is the design of a suitable wave launcher, which generates waves of a specified wavelength spectrum while maximizing the power handling capability. Moreover, care must be taken to protect the radiating elements from the particle and energy fluxes at the plasma periphery and to prevent the unwanted contamination of the plasma by ablation of the antenna materials. In order to ensure the excitation of only the fast wave, a polarization shield, or so-called Faraday shield has commonly been fixed over the radiating element to screen out the electrostatic field components while permitting, in the ideal case, complete penetration of the magnetic fields.

In experiments thus far, wave launchers in the ion cyclotron range of frequencies (ICRF) have been based on inductive loops which rely on sufficient coupling of the near fields of the antenna to the edge plasma.¹ With edge plasma parameters commonly encountered in the experiments, antenna loading impedances of a few ohms are found, which necessitates the use of tuning elements to match the antenna to a transmission line. The Q of the resulting tuned circuit is typically in the range of 10-20 and becomes ultimately the limit to the power handling capability when the reactive voltages involved exceed a breakdown limit.²

In proposed reactor or ignition devices, such as the Compact Ignition Tokamak (CIT), the plasma edge power density is expected to be much larger than in current experiments, requiring additional protection for the antenna. Ideas which have been proposed to afford this protection include the use of close fitting protective limiters or the recessing of the entire antenna in a cavity in the vessel wall.³ With such schemes it becomes necessary to make a quantitative trade-off between additional protection and lower power handling capability due to the loss of coupling.

In previous antenna modelling studies, only relatively idealized geometries have been studied, and few have taken into account the effect of the plasma on the radiating conductors. In this paper we present a method for analyzing antennas of arbitrary cross-section above ground planes of arbitrary shape with finite resistance. Faraday shields have been omitted in this treatment, since their effect on the near-zone inductive fields can be made to be negligible with appropriate design. A further limitation is adopted that only those cases are considered where the vacuum wavelengths are much larger than the transverse dimensions of the system, so that the quasistatic fields are a good approximation to the wave fields. A computational model is developed, the ANTenna DESIGN code (ANDES), and the results are compared with other theoretical works as well as with experimental measurements in vacuum. It should be noted that the antenna current distribution is not assumed, as is usually the case in these studies, but is determined self-consistently as a consequence of the influence of the plasma and other radiating elements. The resulting current distribution is used to determine the maximum electric field strength, which in turn is used to estimate the maximum power handling capability for a given antenna design. The power handling capability is studied as a function of geometric shape factors and edge plasma conditions. Results are presented for various proposed antenna designs including those above a ground plane and in the recessed configuration.

In Sec. II we describe the computational algorithm and compare it to other known solutions as well as to experiment in Sec. III. In Sec. IV we present the results of the study of the recessed antenna concept. The conclusions of this work are drawn in Sec. V.

II. Description of the Algorithm

The essential quantity of the antenna design problem to be determined is the distribution of current in the plane transverse to the direction of current flow. Once this is known, the near-zone fields, loading impedance, and coupling efficiency are readily computed. A schematic diagram of the cross-section of a typical ICRF antenna, such as the one used on the Princeton Large Torus (PLT), is shown in Fig. 1. The current is carried by a driven element and returns through the ground plane. In this work we adopt the realistic limitation that the fields are nearly quasistatic, that is, that the variation of current in the direction transverse to the current flow occurs over a distance much shorter than a wavelength. In this case the variation of the current along the antenna is assumed to be sinusoidal and slowly varying, so that the fields form a nearly TEM wave. This assumption allows for the modelling of the current distribution as a collection of elementary filaments, each of which has a limiting self-inductance and a mutual inductance to other filaments which depends primarily on their spacing. The totality of all the filaments comprises a coupled circuit which may be solved by standard matrix methods. This method is akin to the method of moments and amounts to the solution of an integral equation for the current distribution.⁴ In the remainder of this section we develop the model for an elementary current filament and describe a computational algorithm for the solution of the resulting circuit equations.

In the case of a metallic conducting boundary, the surface is divided into a collection of parallel bars that are a skin depth $\delta = \sqrt{2/\sigma\omega\mu}$ thick and w wide as shown in Fig. 2; w is considered to be sufficiently small so that the current is uniform over the bar cross-section. The resistance of each bar is given by $R = \ell/\sigma w\delta$ and the inductance of each bar is given by

$$L = 2 \times 10^{-7} \ell \left[\ln\left(\frac{2\ell}{\delta+w}\right) + 0.5 \right] \quad , \quad (1)$$

where ℓ is the length of the bar. Also, the mutual inductance to any other bar in vacuum is given by

$$M = 2 \times 10^{-7} \ell \left[\ln\left(\frac{2\ell}{d}\right) - 1 + \frac{d}{\ell} - \left(\frac{d}{\ell}\right)^2 \right] \quad ,$$

where d is the distance between the two bars. These expressions are approximations to the exact formulas,⁵ but for the case of $w, d \ll \ell$ they are found to differ from the exact values by no more than 2%. It is further assumed that all the current carried by the antenna is returned via the ground plane and that there is no variation along the direction of current flow ($k_y = 0$). Such an assumption is tantamount to restricting the region of interest to near a current maximum on the antenna and considering the quasi-static variation of the fields transverse to the current channel at this point. With these assumptions an equivalent circuit model can be constructed with regard to the current distribution among the antenna and ground plane elements, as shown in Fig. 3. To illustrate the method, we omit the plasma for the time being. The resulting matrix equation for the voltages and currents can be written in the form

$$\begin{bmatrix} R_a + j\omega L_a & j\omega M_{12} & \cdot & \cdot & \cdot & j\omega M_{1n} \\ j\omega M_{21} & R_a + j\omega L_a & \cdot & \cdot & \cdot & j\omega M_{2n} \\ \cdot & \cdot & \cdot & \cdot & \cdot & \cdot \\ \cdot & \cdot & \cdot & \cdot & \cdot & \cdot \\ \cdot & \cdot & R_g + j\omega L_g & \cdot & \cdot & \cdot \\ j\omega M_{n1} & \cdot & \cdot & \cdot & R_g + j\omega L_g & \cdot \end{bmatrix} \begin{bmatrix} I_1 \\ I_2 \\ \cdot \\ \cdot \\ I_{n-1} \\ I_n \end{bmatrix} = \begin{bmatrix} V_a \\ V_a \\ \cdot \\ \cdot \\ V_g \\ V_g \end{bmatrix}$$

or

$$[Z] [I] = [V] \quad ,$$

where $[Z]$ is the $n \times n$ impedance matrix which is complex symmetric, $[I]$ is the current vector, and $[V]$ is the voltage vector. To solve for $[I]$, $[Z]$ is inverted with $[Y] = [Z]^{-1}$ and we require that the sum of the driving currents plus the return currents sum to 0, i.e.,

$$I_a = \sum_{i=1}^m I_i = 1, \quad \text{and}$$

$$I_g = \sum_{i=m+1}^n I_i = -1 \quad ,$$

where we chose m -driven antenna elements and $n-m$ ground plane elements. Since the voltages across parallel elements are equal, the matrix can be broken down into smaller partial matrices and solved as follows:

$$\begin{bmatrix} A & B \\ C & D \end{bmatrix} \begin{bmatrix} V_a \\ V_g \end{bmatrix} = \begin{bmatrix} I_a \\ I_g \end{bmatrix} = \begin{bmatrix} 1 \\ -1 \end{bmatrix} \quad ,$$

where

$$A = \sum_{i=1}^m \sum_{j=1}^m Y_{ij}$$

$$B = \sum_{i=1}^m \sum_{j=m+1}^n Y_{ij}$$

$$D = \sum_{i=m+1}^n \sum_{j=m+1}^n Y_{ij}$$

$C = B$ by symmetry. From these partial matrices V_a and V_g may be solved directly:

$$V_g = \frac{1}{B - A\left(\frac{B+D}{A+B}\right)}$$

$$V_a = -\frac{(B+D)}{(A+B)} V_g .$$

Once these voltages are known, both the current distribution and the input impedance can be determined. The total dissipated power is further determined from the real part of the input impedance, as is the antenna Q , defined to be the ratio of the input reactance to the input resistance.

The main purpose of this work is to evaluate the coupling of various antenna configurations in the presence of plasma. To this end, it is necessary to construct a representation for the plasma surface impedance in terms of the filament model described above. However, it is most convenient to represent the plasma impedance in Fourier space (k_z) where the Fourier transform is taken in the direction along a field line, as shown in Fig. 2. For the purposes of this study, we assume the plasma is completely absorbing at infinity, so that only an outgoing wave may be retained in the plasma halfspace. This is a good assumption for most cases expected in both current and future ICRF experiments.⁶ On the vacuum side, the fields have the form

$$E_y = c_1 \exp(-ikx)$$

$$H_z = \frac{1}{i\omega\mu} \frac{\partial E_y}{\partial x} = \frac{-k}{\omega\mu} c_1 \exp(-ikx)$$

with: $k = \sqrt{k_0^2 - k_z^2}$ $k_0^2 = \omega^2/c^2$

and on the plasma side we have:

$$E_y = c_2 \exp(ik_x x)$$

$$H_z = \frac{k_x c_2}{\omega \mu} \exp(ik_x x)$$

$$\text{with: } k_x^2 = \frac{(k_o^2 K_{\perp}^2 - k_z^2)^2 + k_o^4 K_x^2}{k_o^2 K_{\perp}^2 - k_z^2} ,$$

where for the range of frequencies of interest

$$K_{\perp}^2 \approx \frac{\omega_{pi}^2}{c^2} \frac{\omega^2}{\omega - \omega_{ci}^2}$$

$$K_x^2 \approx \frac{\omega}{\omega_{ci}^2} K_{\perp}^2 ,$$

and ω_{pi} is the ion plasma frequency and ω_{ci} is the ion cyclotron frequency.

At the plasma element ($x = 0.0$, $z = z_o$), we assume that E_y is continuous and that H_z has the jump of I_o/w , therefore:

$$c_1 = c_2$$

$$\frac{k_x c_2}{\omega \mu} = \frac{-c_1 k}{\omega \mu} + \frac{I_o}{w} .$$

This yields:

$$c_1 = c_2 = \frac{\omega \mu}{(k + k_x)} \frac{I_o}{w}$$

$$E_y(x = 0.0) = \frac{\omega \mu}{(k + k_x)} \frac{I_o}{w} .$$

The power flowing in the element is:

$$P = l/2 \int_{-\infty}^{\infty} E_y J_y^* dz$$

We assume that the current is uniform across the strip ($J_y w = I_0$). We find the Fourier representation for J_y and E_y :

$$\begin{aligned} J_{y,k} &= \int_{-\infty}^{\infty} J_y e^{-ikz} dz \\ &= J_y L \frac{\sin(k w/2)}{k w/2} \\ &= I_0 \frac{\sin(k w/2)}{k w/2} \end{aligned}$$

and similarly

$$E_{k,x} = \frac{\omega \mu}{(k + k_x)} \frac{I_0 \sin(k w/2)}{k w/2}$$

Using Parseval's theorem, the power is

$$P = \frac{l}{2} \frac{1}{2\pi} \int_{-\infty}^{\infty} E_k J_{-k}^* dk_z$$

and the impedance

$$Z = \frac{P}{I_0} = \frac{l \omega \mu}{\pi w} \int_{-\infty}^{\infty} \frac{\sin^2(k w/2)}{(k_x + k) k_z} dk_z$$

In a similar way, the mutual impedance can be found

$$Z(z, z_0) = \frac{P}{I_0^2} = \frac{2\omega\mu}{\pi w} \int_0^\infty \frac{\sin^2(k_z w/2)}{(k_x + k)k_z} e^{-ik_z(z-z_0)} dk_z .$$

For the region of interest for this problem we may take $k_0 \neq 0$ and $k = ik_z$. The impedance for a typical case is shown in Fig. 4. It is noted that the mutual resistance between two plasma elements can be negative, a manifestation of the relatively short wavelength which exists in the presence of plasma. A similar result is obtained for the mutual impedance of dipole antennas.⁷ The essence of the coupling problem is contained in the impedance of the plasma elements. The presence of plasma converts the pure inductive mutual impedance seen between vacuum elements into a complex mutual impedance, i.e., the antenna near zone fields become propagating waves and have real power flow once they have penetrated the plasma surface.

The plasma elements are incorporated into the circuit model in the same manner that the ground plane elements are handled. In particular, the boundary condition used is that the sum of all the plasma surface currents is zero. This condition forces a current reversal in the plasma plane, as expected. Figure 5 indicates the magnitude and phase of the surface currents in the plasma for a typical case. We note that the phase variation represents a traveling wave emanating from the antenna along the plasma surface. Also, due to the finite extent of the domain, some reflection of the waves is observed at the ends of the domain. This is an artifact of the abrupt change in surface impedance at this point suggesting that for sufficient accuracy, the domain must be taken to be sufficiently large so that most of the power has radiated into the plasma before encountering the ends. In the next section we benchmark this model against both simple analytical models and experimental measurements.

III. Comparison with Analytical Results and Experimental Measurements

As a check on the algorithm, we first consider the case of a thin current strip above an infinite ground plane whose analytical solution is known.⁸ The limit is taken where the antenna dimensions are short with respect to a wavelength so that the expression for the low frequency inductance is appropriate. In the case of a TFR antenna analyzed by Adam,⁹ as shown in Fig. 6(a), the inductance using the analytical solution is found to be 2.47×10^{-9} henrys/meter. Adam found the inductance of this antenna by first Fourier analyzing the fields between the antenna and the ground plane and then integrating over Fourier space to determine the total stored field energy. The resulting inductance is derived directly from stored energy and is found to agree well with the analytic result. The results from ANDES give a similar value of 2.3×10^{-9} henrys/meter. The current distribution in this calculation was not assumed to be uniform, as in Adam's work, but is found to be peaked near the ends of the conductor, as shown in Fig. 6(b). This slightly lower value is consistent with minimization of the stored energy as the actual current distribution is approached.

Further confirmation of the model has been made by comparison with the experimental measurements of Fortyang and Hwang for the PLT antenna in vacuum.¹⁰ In their work, a small current probe was used to measure the near-zone fields in the vicinity of a PLT antenna. Figure 7 shows the comparison between the measured values and the results from ANDES, indicating excellent agreement in both directions transverse to the current flow. It is worthy to note that in order to achieve this agreement, the flux had to be integrated over an area equal to the probe aperture, even though this was small, indicating the current distribution may be more peaked than actually

measured. Figure 8 shows ANDES predicted current distribution for the PLT antenna. Notice that current tends to be excluded from the interior corners and peaks on the lobes of the antenna. Also, current tends to be greater on the surface furthest from the ground plane.

The comparison of ANDES with experimental results in the presence of plasma is complicated by the fact that the experimental edge density profiles are not well known. The real part of the antenna impedance has been shown to be a sensitive function of the edge density and the distance between the antenna and the plasma. For the purposes of this study, we have assumed a uniform plasma density with a fixed separation from the antenna (independent of k_z). By comparison, Adam assumed parabolic edge density profiles and allowed the separation distance to be a function of k_z in order to model the variable evanescent distance expected in the presence of gradients. Since the presence of plasma is not found to affect the antenna reactance appreciably, we do not expect the details of the plasma edge to affect the current distributions significantly. The antenna resistance or coupling coefficient is affected, however, and we adjust the edge parameters to fit experimentally measured values.

In accord with the measurements of Fortgang and Hwang, a reduction of the overall coupling impedance of 50% should be made to account for the decrease of the antenna current away from the current maximum (i.e., due to the finite wavelength along the antenna length). In the PLT case, an edge density of $1 \times 10^{12} \text{ cm}^{-3}$ is sufficient to reproduce the 3 ohm loading impedances found in the experiments. Using this value, the results from ANDES for the PLT antenna and related variations of this antenna are shown in Table 1. These results do not take into account the expected reduction in input impedance and are presented for comparison of various antenna designs. The input impedance

predicted by ANDES for the PLT antenna of 6 ohms should translate to an experimentally observed input impedance of about 3 ohms, in agreement with the experiment.

Table 1 indicates that the peak electric field on the antenna surface (i.e., the antenna Q) can be lowered by increasing the antenna width and thickness. As the antenna is made wider, the magnetic flux concentration at the ground plane increases and the input impedance decreases. Table 1 shows that the peak electric field at the antenna surface for the case of 1 MW delivered power into the plasma can be reduced by 30% just by increasing the antenna thickness to 2 cm. Results also show that the input impedance can be appreciably increased by increasing the distance between the antenna and the ground plane. In the next section we apply this model to determine optimal conductor to ground plane spacing for lowering the peak electric fields and to ascertain the coupling for more complicated geometries.

IV. Application of the Model to Recessed Antenna Coupling

The main motivation for this work is to study recessed antenna configurations and determine if this scheme can provide effective plasma heating. An antenna of round cross section in a semi-circular recess was investigated because it was believed that this would distribute the current more evenly across the antenna surface. Results showed that this configuration did have well-distributed current, but to achieve a comparatively low electric field required antennas of relatively large radius in a recess of equally large radius.

In order to restrict the analysis to a small number of physically realizable configurations, we shall focus our study on rectangular recesses

with rounded corners. We present the results for the case of two different channel depths. Referring to Fig. 9, a 14 cm wide and 2 cm thick antenna depressed 1.5 cm in a recess was analyzed. The channel width was varied from 15 cm to a width such that the channel could be viewed as a flat ground plane. The plasma was 3 cm in front of the recess and the density was $5 \times 10^{12} \text{ cm}^{-3}$. These are expected to be in accord with the requirements of the CIT. The predicted input resistance and electric field for a 5 cm and 10 cm deep channel are shown in Fig. 10.

We calculated the peak electric field for each antenna configuration delivering 1 MW into the plasma. As shown in Fig. 11, the noteworthy result is observed that the total electric field at the antenna reached a minimum when the channel width was made about 2.5 times the antenna width. Adequate input resistances for coupling in the range of ($> 2 \Omega$) are found for these configurations at these channel widths as well. From these results we believe that there is no need for extremely wide channels. Sufficient loading and relatively low electric fields should be obtainable without imposing unrealistic constraints on the size of the launching structure.

The Fourier spectrum of the antenna fields can be determined by a direct evaluation of the Fourier integral using the results of the previous calculation. For comparison purposes the spectrum of the B_z component of the RF field is evaluated along a layer just above the ground plane. The limits of the Fourier integral, which determine the minimum Δk_z resolution of the spectrum, were found to be sufficient at ± 5 times the channel width.

Figure 12a is a typical spectrum for the recessed configuration. The location of the minor peak in the spectrum is determined by the channel width, while the location of the major peak is determined by the assumed edge plasma density. The latter feature is essentially the same for both the recessed and

nonrecessed configurations and reflects the significance of the plasma edge in determining the ground plane currents. It is worthwhile to note that the width of the driven element itself has a minimal effect on the spectrum in the recessed configuration.

The Fourier spectrum of an identical antenna for the nonrecessed configuration, evaluated along a layer just above the antenna surface, is shown in Fig. 12b. The spectra in Fig. 12 are very similar, indicating the dominant spectral filtering imposed by the plasma surface. This implies that the plasma edge density is the most important factor governing the character of the launched wave spectrum.

V. Conclusions

Results from ANDES compared to experimental results suggest that we can accurately model antennas of arbitrary cross section above a ground plane. From these results we believe that this analysis applied to recessed antennae is valid and will be useful in predicting coupling for ICRF heating. The results of this analysis indicate that the recessed configuration can be expected to provide adequate coupling for ICRF heating applications. A fully three-dimensional analysis considering variation of current along the antenna would provide a more complete treatment of the problem, but this analysis would undoubtedly require large amounts of computer time and would not appreciably change the character of the results for antennas whose transverse dimensions are small with respect to a wavelength. A density gradient was not considered in this analysis and may modify the absolute value of the loading impedance but not the relative scaling of the impedance with geometric factors.

Acknowledgments

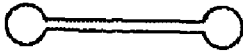



One of the authors (ISL) would like to acknowledge C.C. Paulson for his helpful suggestions and discussions concerning the ANDES code. This work is supported by Grumman Aerospace Corporation and the Department of Energy Contract # DE-AC02-76-CWO-3073.

References

- 1 J.R. Wilson, "Experimental Topics in ICRF Heating of Toroidal Plasmas," Course and Workshop on Applications of RF Waves to Tokamak Plasmas, Varenna, Italy (1985).
- 2 J.H. Mullen and J.W. Davis, "High Power ICRH Launcher Development," IEEE Trans. Plasma Sci., Vol. PS-12, No. 2, (June 1984) p. 79.
- 3 CIT ICRF Design Group, CIT Conceptual Design Report, Princeton Plasma Physics Laboratory, 1986.
- 4 W.K. Stutzman and G.A. Thiele, Antenna Theory and Design, (Wiley, NY, 1981) p. 306.
- 5 F.W. Grover, Inductance Calculations, Formula and Tables, (D. Van Nostrand Company, NY, 1946) pp. 34-35.
- 6 P. Colestock, "Review of ICRF Experiments," IEEE Trans. Plasma Sci., Vol. PS-12, No. 2 (June 1984) p. 64.
- 7 J.D. Kraus, Antennas, (McGraw Hill, NJ, 1950) p. 266.
- 8 F.W. Grover, Inductance Calculations, Formula and Tables, (D. Van Nostrand Company, NY, 1946) p. 40.
- 9 J. Adam, "Cyclotronic Heating Antenna Impedance in the presence of Powerful Absorption," Oak Ridge National Laboratory Report No. ORNL OLS-82-29, (1979).
- 10 C.M. Fortgang and D.Q. Hwang, "Measurements of the Electrostatic and Electromagnetic Fields of Faraday Shielded Half-Turn Loop Type ICRF Antennae," Princeton Plasmas Physics Laboratory Report No. PPPL-2183 (1984).

Table 1

86X0738

	<u>Maximum Electric Field</u> (V / cm.-amp)	<u>Input Resistance</u> (ohms)	<u>Electric Field at 1Megawatt</u> (kV / cm.)
(A) 	58.6	6.0	21.2
(B) 	40.0	5.9	14.1
(C) 	28.6	5.5	10.3
(D) 	16.6	4.4	7.2

Four different antenna shapes drawn to relative scale are compared for the case of a 1.3 meter long antenna in the presence of a plasma with $n = 1 \times 10^{12} \text{ cm}^{-3}$. The total peak electric field is calculated for the case of 1 MW delivered into the plasma. Shape A is the present PLT antenna.

Figure Captions

Fig. 1. Schematic diagram of the PLT fast wave antenna with partial Faraday shield.

Fig. 2. Conceptual design of a recessed antenna for the Compact Ignition Tokamak. Expanded view shows the division of elements used to model the antenna. The magnetic field, B , is taken to be along the z direction.

Fig. 3. Circuit model of the antenna and ground plane. V_a is the voltage across the antenna and V_g is the voltage across the ground plane. R_a , L_a and R_g , L_g represent the resistance and inductance of the antenna and ground plane elements, respectively. M represents the mutual inductance between elements.

Fig. 4. a) Real part of the mutual impedance of one plasma element to another. b) Imaginary part of the mutual impedance. Δ is the separation of the elements, $\Delta = 0$ corresponds to an element's self-impedance. This case was for a plasma element 1 meter long with a density of $1 \times 10^{12} \text{ cm}^{-3}$.

Fig. 5. a) Magnitude of the current flowing in the plasma elements; b) phase of the current.

Fig. 6. a) Schematic diagram of the ICRF antenna analyzed by Adam in the presence of plasma. The antenna is 1 meter long, 6 cm wide and 2 cm above the ground plane in the presence of a plasma with $n = 1 \times 10^{12} \text{ cm}^{-3}$; a few field lines are shown. b) current distribution along the surface of the antenna as predicted by ANDES.

Fig. 7. a) Measurement of magnetic flux (solid dots) across the top surface of the PLT antenna plotted against the predicted flux by ANDES; b) measurement of magnetic flux in a direction perpendicular to the top surface and ANDES predicted result.

Fig. 8. ANDES predicted current distribution for the PLT antenna. The antenna is 5 cm above a ground plane.

Fig. 9 CIT antenna in the presence of plasma with $n = 5 \times 10^{12} \text{ cm}^{-3}$; a few field lines are shown. A 14 cm wide, 2 cm thick antenna depressed 1.5 cm was analyzed for different channel widths and depths.

Fig. 10. Predicted input resistance and electric field for a 1 meter length antenna as in Fig. 9 in the presence of plasma. a) 5 cm depth channel; b) 10 cm depth channel.

Fig. 11. Peak electric field for the CIT antenna delivering 1 megawatt into the plasma, results for a 5 cm depth and 10 cm depth channel as in Fig. 9.

Fig. 12. (a) Fourier spectrum of the B_z component of the RF field for the recessed configuration.

(b) Fourier spectrum for the nonrecessed configuration.

86X1031

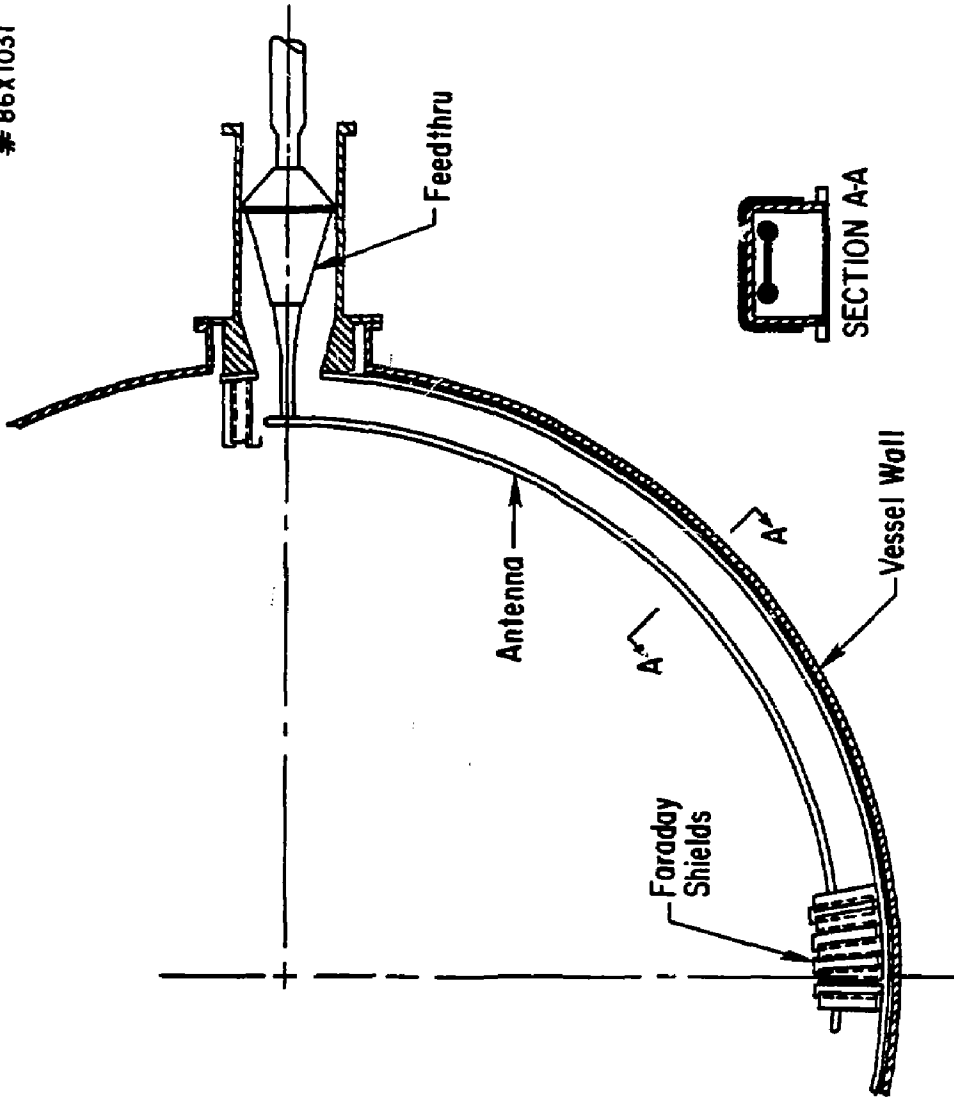


Fig. 1

#86X0736

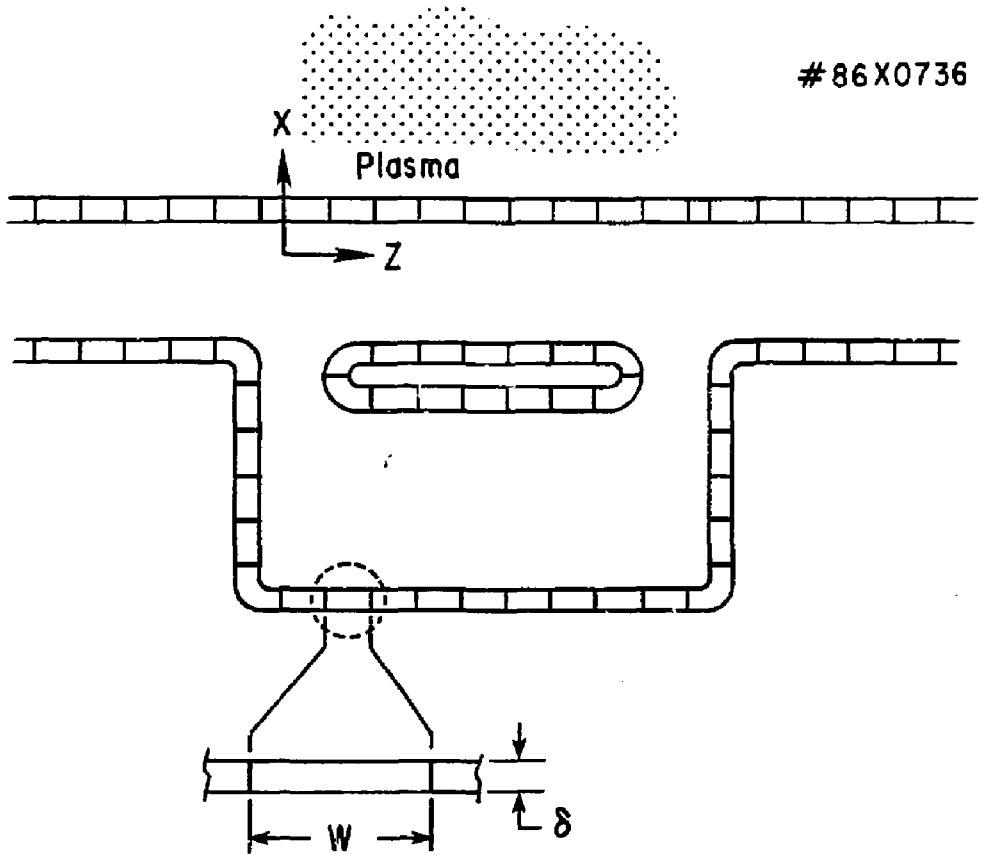


Fig. 2

#86X0737

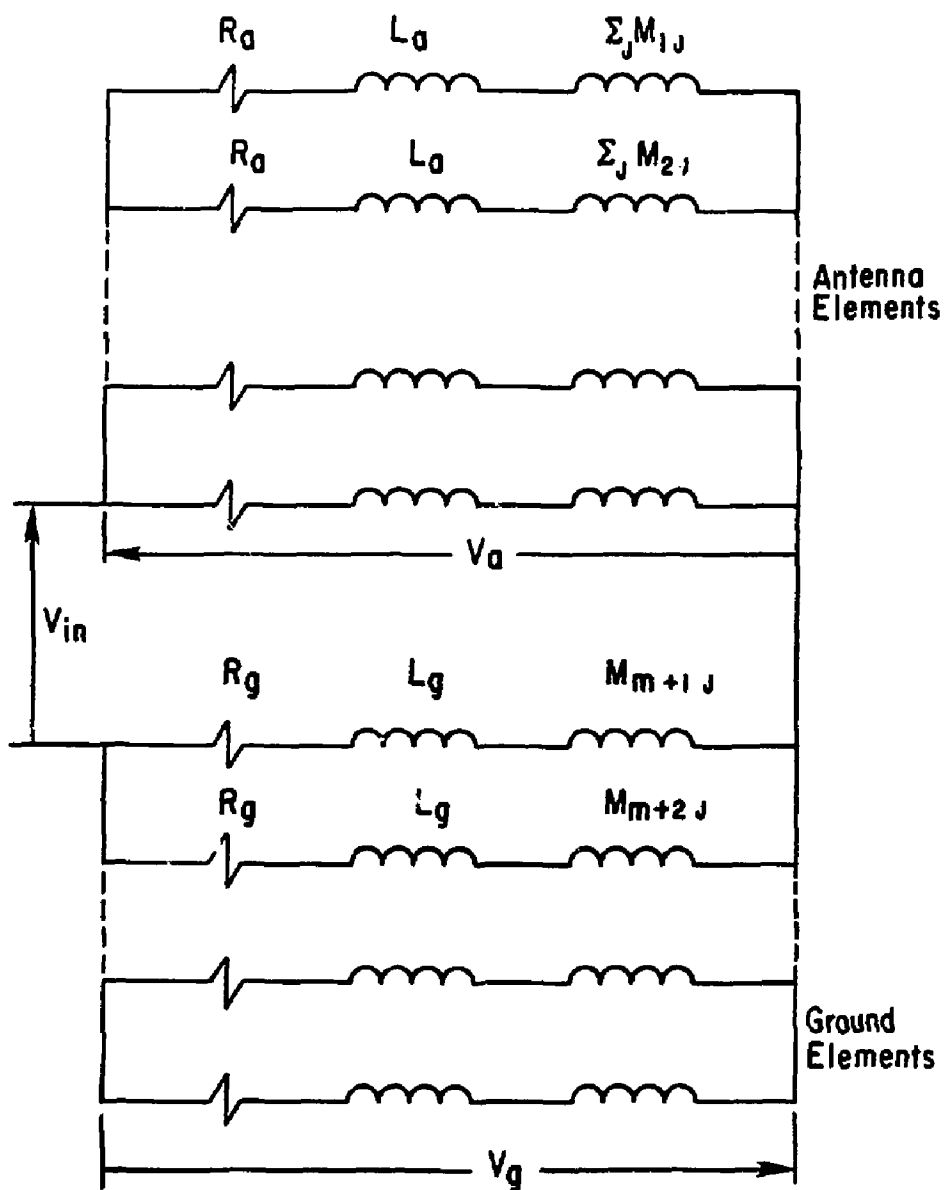


Fig. 3

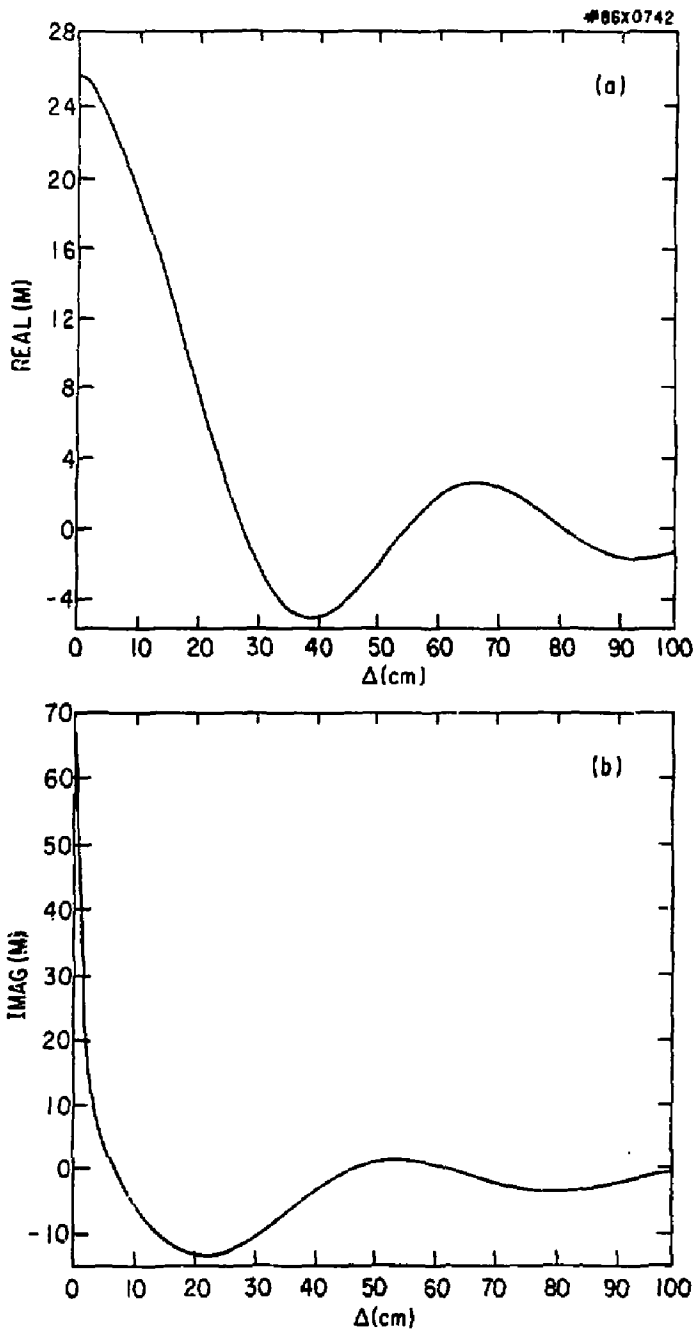


Fig. 4

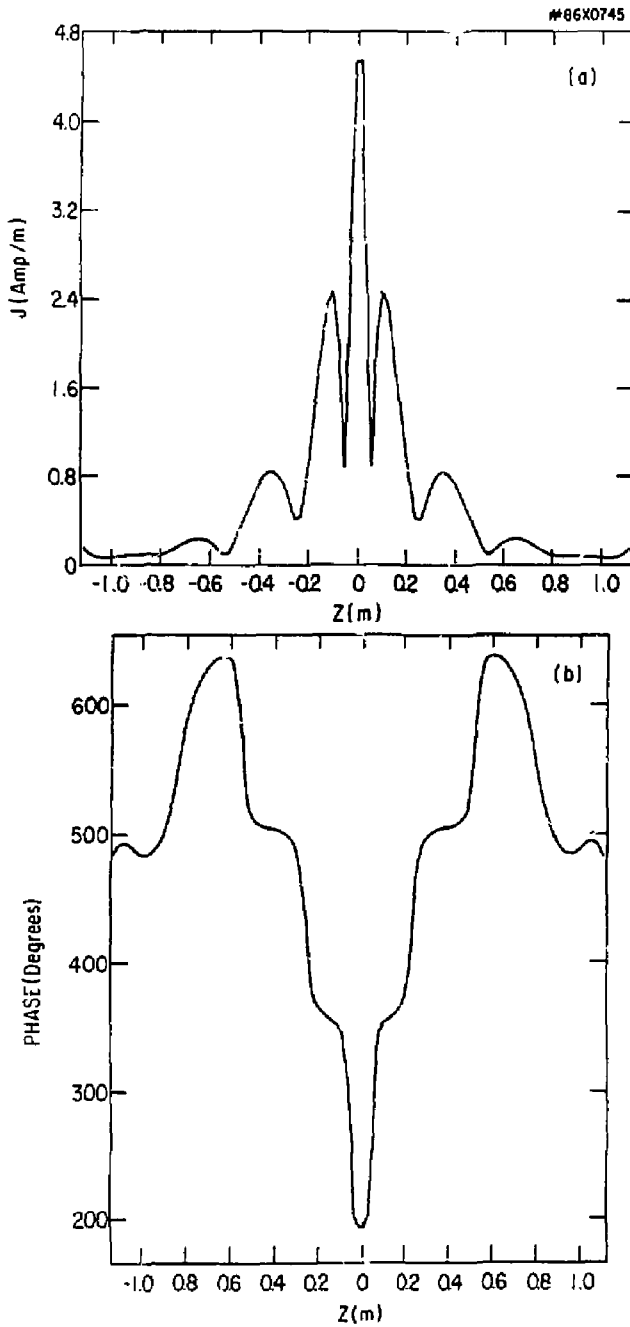


Fig. 5

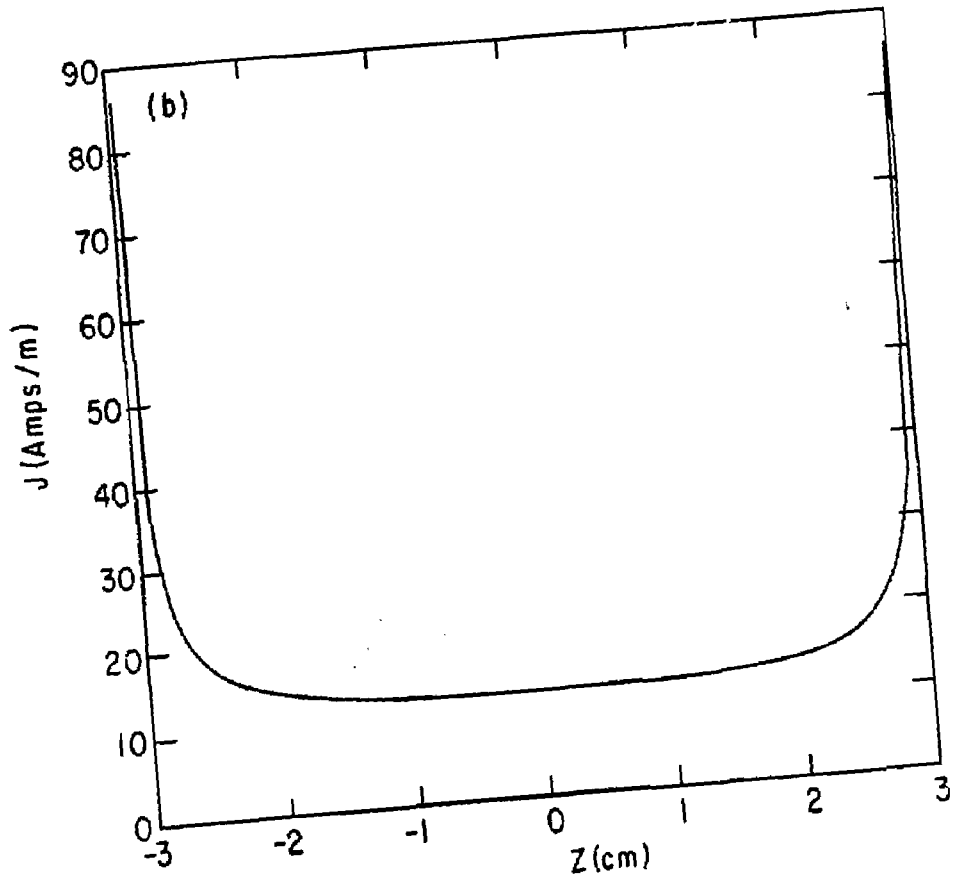
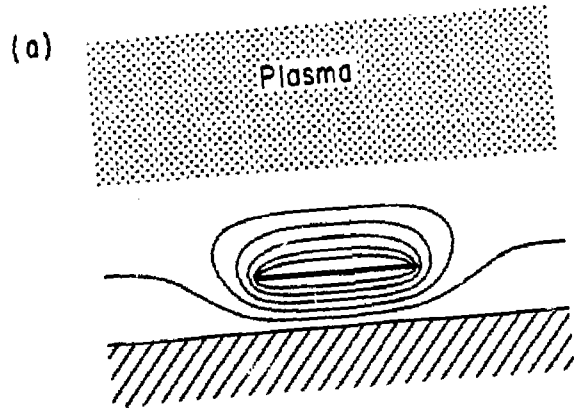


Fig. 6

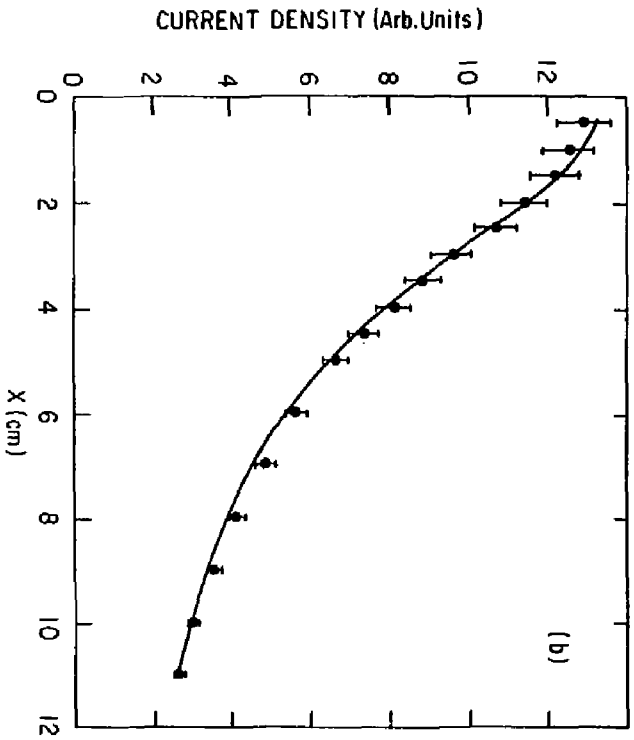
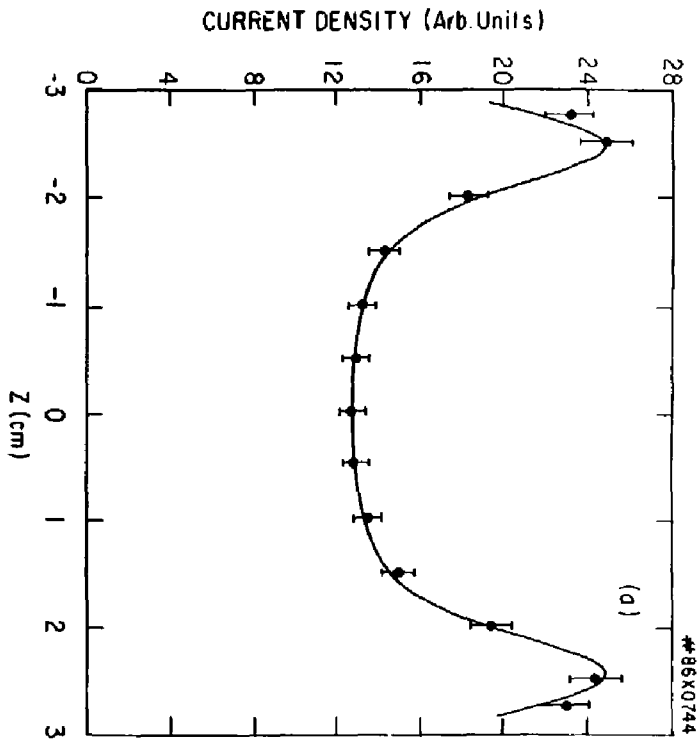


Fig. 7

#86X0740

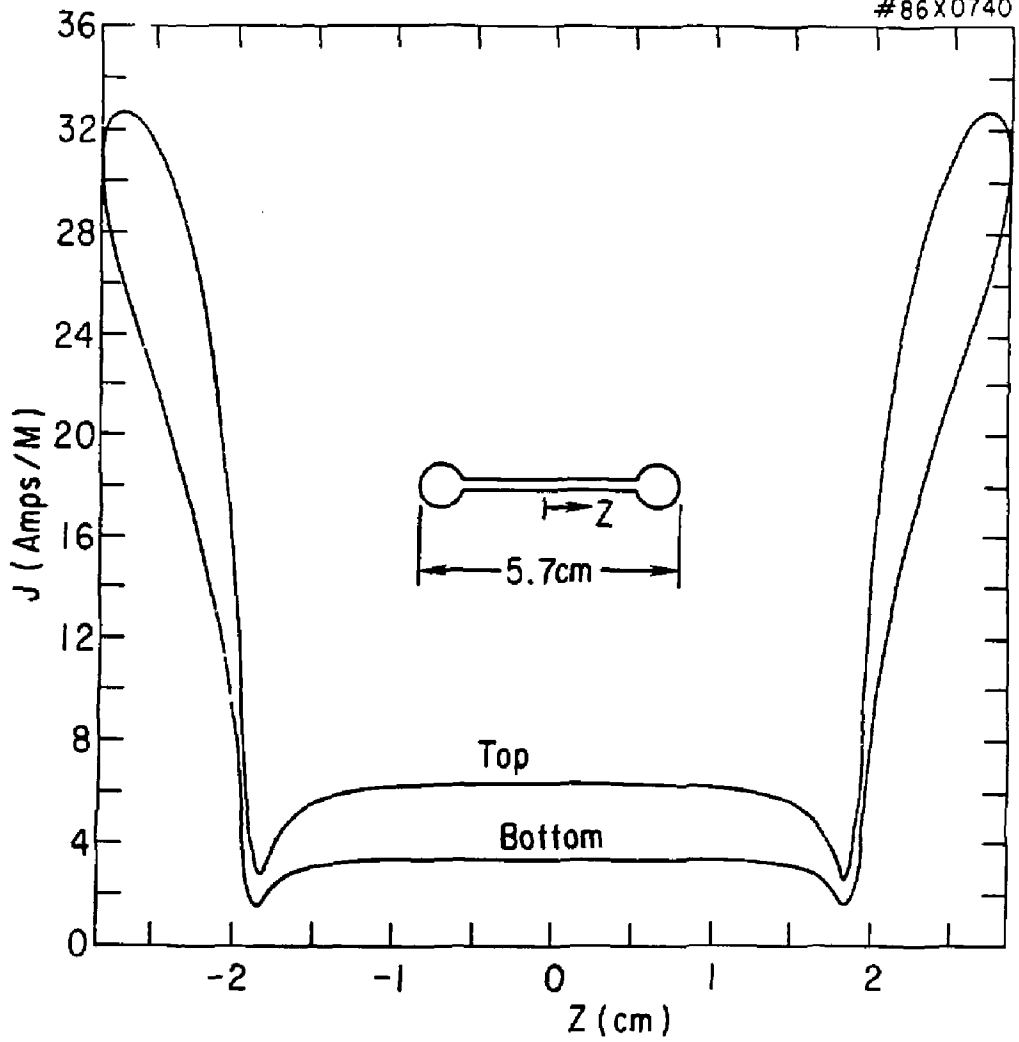


Fig. 8

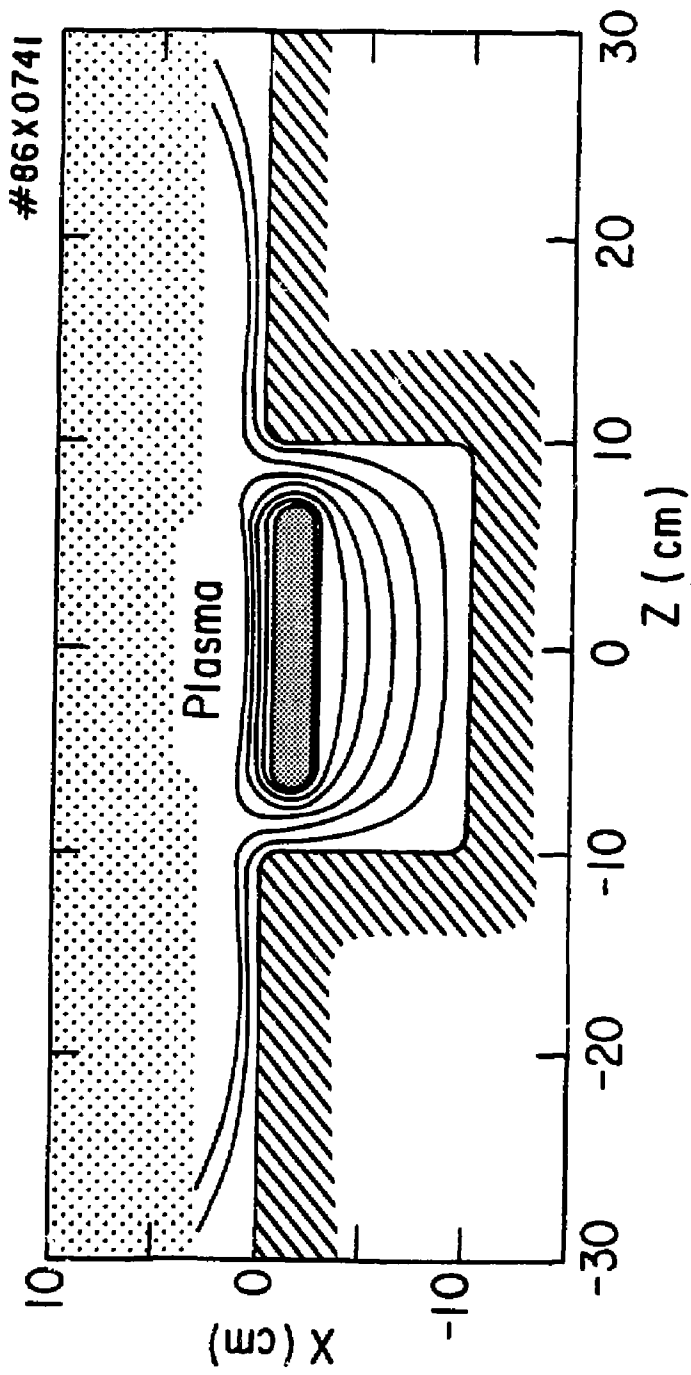


Fig. 9

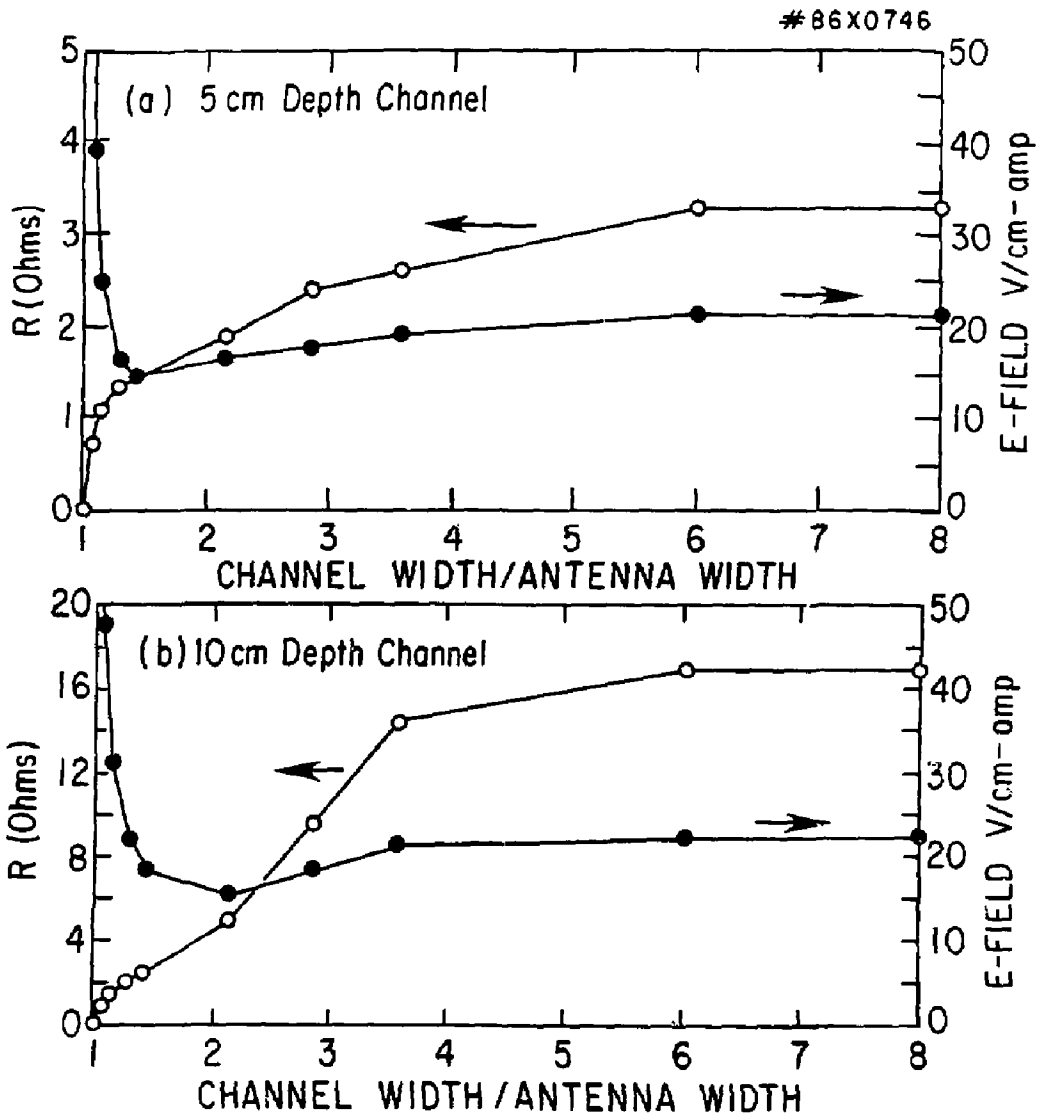


Fig. 10

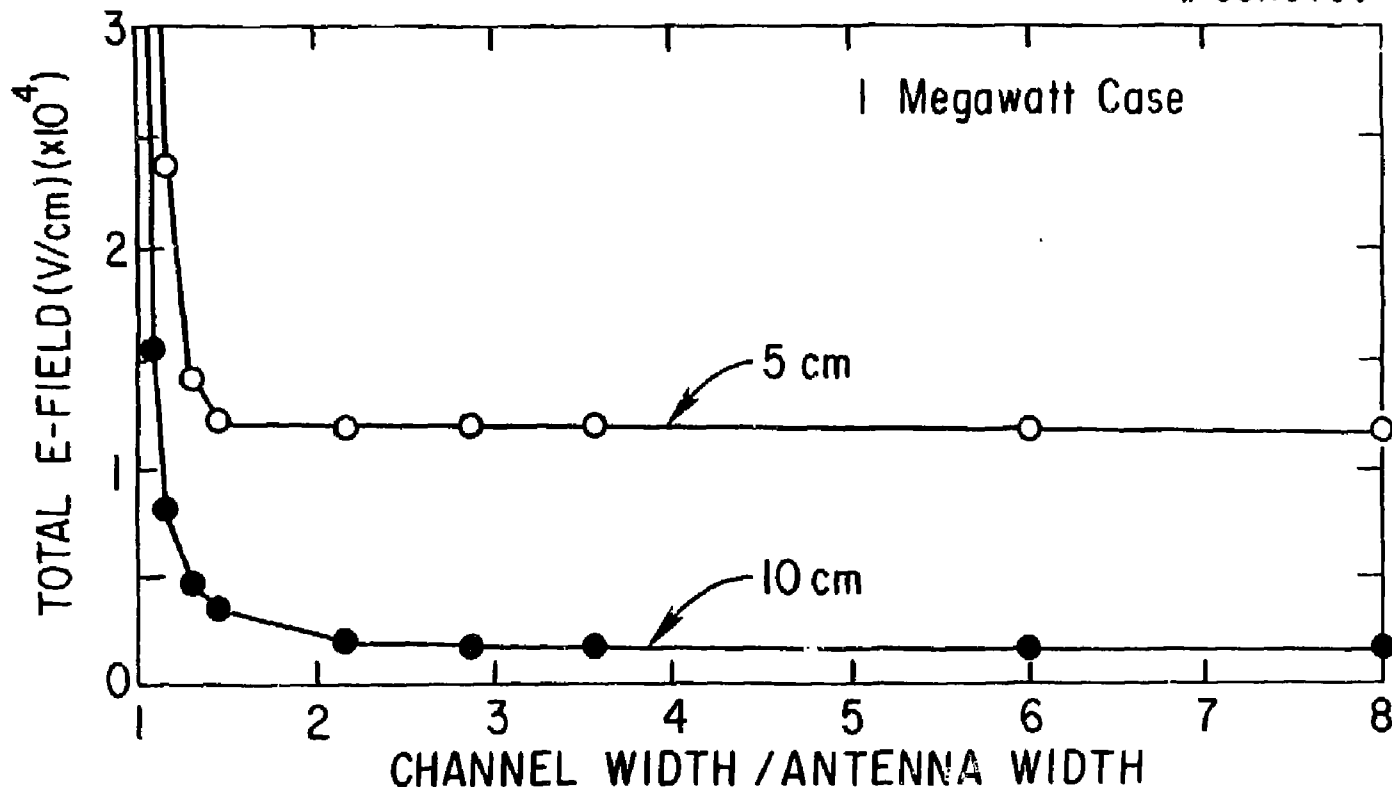


Fig. 11

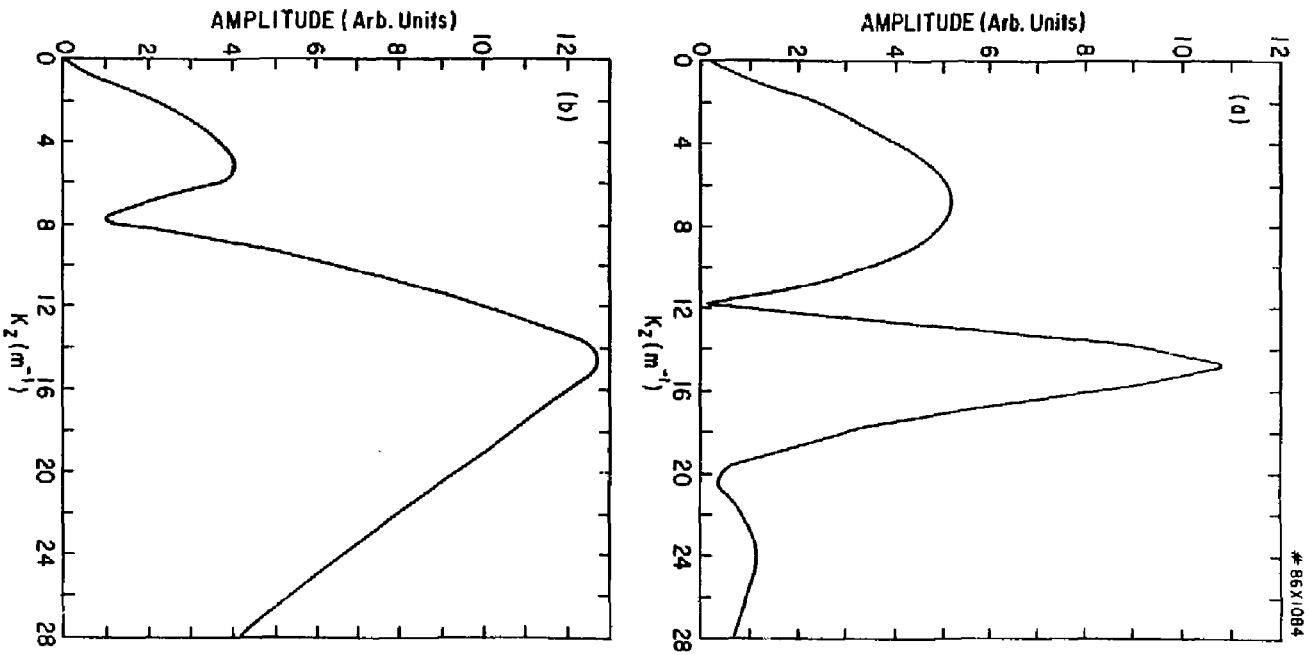


Fig. 12

EXTERNAL DISTRIBUTION IN ADDITION TO UC-20

Plasma Res Lab, Austr Nat'l Univ, AUSTRALIA
Dr. Frank J. Paoloni, Univ of Wollongong, AUSTRALIA
Prof. I.R. Jones, Flinders Univ., AUSTRALIA
Prof. M.H. Brennan, Univ Sydney, AUSTRALIA
Prof. F. Cap, Inst Theor Phys, AUSTRIA
M. Goossens, Astronomisch Instituut, BELGIUM
Prof. R. Boucique, Laboratorium voor Natuurkunde, BELGIUM
Dr. D. Palumbo, Dg XII Fusion Prog, BELGIUM
Ecole Royale Militaire, Lab de Phys Plasmas, BELGIUM
Dr. P.H. Sakanaka, Univ Estadual, BRAZIL
Lib. & Doc. Div., Instituto de Pesquisas Especiais, BRAZIL
Dr. C.R. James, Univ of Alberta, CANADA
Prof. J. Teichmann, Univ of Montreal, CANADA
Dr. H.M. Skarsgard, Univ of Saskatchewan, CANADA
Prof. S.R. Sreenivasan, University of Calgary, CANADA
Prof. Tudor W. Johnston, INRS-Energie, CANADA
Dr. Hannes Barnard, Univ British Columbia, CANADA
Dr. M.P. Bachynski, MPB Technologies, Inc., CANADA
Chalk River, Nucl Lab, CANADA
Zhengwu Li, Sw Inst Physics, CHINA
Library, Tsing Hua University, CHINA
Librarian, Institute of Physics, CHINA
Inst Plasma Phys, Academia Sinica, CHINA
Dr. Peter Lukac, Komenského Univ, CZECHOSLOVAKIA
The Librarian, Culham Laboratory, ENGLAND
Prof. Schatzman, Observatoire de Nice, FRANCE
J. Radet, CEN-BP6, FRANCE
JET Reading Room, JET Joint Undertaking, ENGLAND
AM Dupas Library, AM Dupas Library, FRANCE
Dr. Tom Muoi, Academy Bibliographic, HONG KONG
Preprint Library, Cent Res Inst Phys, HUNGARY
Dr. R.K. Chhajlani, Vikram Univ, INDIA
Dr. B. Dasgupta, Sahe Inst, INDIA
Dr. P. Kew, Physical Research Lab, INDIA
Dr. Phillip Rosenau, Israel Inst Tech, ISRAEL
Prof. S. Cuperman, Tel Aviv University, ISRAEL
Prof. G. Rostagni, Univ Di Padova, ITALY
Librarian, Int'l Ctr Theo Phys, ITALY
Miss Ciella De Palo, Assoc EURATOM-ENEA, ITALY
Biblioteca, del CNR EURATOM, ITALY
Dr. H. Yamato, Toshiba Res & Dev, JAPAN
Dirac, Dept. Lg. Tokamak Dev. JAERI, JAPAN
Prof. Nobuyuki Inoue, University of Tokyo, JAPAN
Research Info Center, Nagoya University, JAPAN
Prof. Kyoji Nishikawa, Univ of Hiroshima, JAPAN
Prof. Sigeru Mori, JAERI, JAPAN
Prof. S. Tanaka, Kyoto University, JAPAN
Library, Kyoto University, JAPAN
Prof. Ichiro Kawakami, Nihon Univ, JAPAN
Prof. Satoshi Itoh, Kyushu University, JAPAN
Dr. D.I. Choi, Adv. Inst Sci & Tech, KOREA
Tech info Division, KAERI, KOREA
Bibliotheek, Fom-Inst voor Plasma, NETHERLANDS
Prof. B.S. Lilly, University of Waikato, NEW ZEALAND
Prof. J.A.C. Cabral, Inst Superior Tecn, PORTUGAL
Dr. Octavian Petrus, ALI CUZA University, ROMANIA
Prof. M.A. Hellberg, University of Natal, SO AFRICA
Dr. Johan de Villiers, Plasma Physics, Nucor, SO AFRICA
Fusion Div. Library, JEN, SPAIN
Prof. Hans Wilhelmson, Chalmers Univ Tech, SWEDEN
Dr. Lennart Stenflo, University of UMEA, SWEDEN
Library, Royal Inst Tech, SWEDEN
Centre de Recherches, Ecole Polytech Fed, SWITZERLAND
Dr. V.T. Tolok, Kharkov Phys Tech Ins, USSR
Dr. D.D. Ryutov, Siberian Acad Sci, USSR
Dr. G.A. Eliseev, Kurchatov Institute, USSR
Dr. V.A. Glukhikh, Inst Electro-Physical, USSR
Institute Gen. Physics, USSR
Prof. T.J.M. Boyd, Univ College N Wales, WALES
Dr. K. Schindler, Ruhr-Universität, W. GERMANY
ASDEX Reading Rm, IPP/Max-Planck-Institut für
Plasmaphysik, F.R.G.
Nuclear Res Estab, Julich Ltd, W. GERMANY
Librarian, Max-Planck Institut, W. GERMANY
Bibliothek, Inst Plasmaforschung, W. GERMANY
Prof. R.K. Janev, Inst Phys, YUGOSLAVIA

NOTICE

This report was prepared as an account of work sponsored by the United States Government. Neither the United States nor the United States Department of Energy, nor any of their employees, nor any of their contractors, subcontractors, or their employees, makes any warranty, express or implied, or assumes any legal liability or responsibility for the accuracy, completeness or usefulness of any information, apparatus, product or process disclosed, or represents that its use would not infringe privately owned rights.

Printed in the United States of America

Available from:

National Technical Information Service
U.S. Department of Commerce
5285 Port Royal Road
Springfield, Virginia 22161

Price Printed Copy \$ * ; Microfiche \$4.50

<u>*Pages</u>	<u>NTIS Selling Price</u>
1-25	\$7.00
25-50	\$8.50
51-75	\$10.00
76-100	\$11.50
101-125	\$13.00
126-150	\$14.50
151-175	\$16.00
176-200	\$17.50
201-225	\$19.00
226-250	\$20.50
251-275	\$22.00
276-300	\$23.50
301-325	\$25.00
326-350	\$26.50
351-375	\$28.00
376-400	\$29.50
401-425	\$31.00
426-450	\$32.50
451-475	\$34.00
476-500	\$35.50
500-525	\$37.00
526-550	\$38.50
551-575	\$40.00
576-600	\$41.50

For documents over 600 pages, add \$1.50 for each additional 25-page increment.